



An Optimum Selection of Simulated Geological Models by Multi-Point Geostatistics and Multi-Criteria Decision-Making Approaches; a Case Study in Sungun Porphyry-Cu deposit, Iran

S. Talesh Hosseini¹, O. Asghari^{1*}, S.A. Torabi² and M. Abedi³

1- Simulation and Data Processing Laboratory, School of Mining Engineering, College of Engineering, University of Tehran, Tehran, Iran.

2- School of Industrial Engineering, College of Engineering, University of Tehran, Tehran, Iran.

3-Geo-Exploration Targeting Laboratory (GET-Lab), School of Mining Engineering, College of Engineering, University of Tehran, Tehran, Iran.

Received 19 July 2019; received in revised form 20 February 2020; accepted 21 February 2020

Keywords

Sophisticated geological units

Training image

SNESIM algorithm

Multi-criteria decision-making

Sungun Porphyry-Cu Deposit.

Abstract

An accurate modeling of sophisticated geological units has a substantial impact on designing a mine extraction plan. Geostatistical simulation approaches, via defining a variogram model or incorporating a training image (TI), can tackle the construction of various geological units when a sparse pattern of drilling is available. The variogram-based techniques (derived from two-point geostatistics) usually suffer from reproducing complex and non-linear geological units as dyke. However, multipoint geostatistics (MPS) resolves this issue by incorporating a training image from a prior geological information. This work deals with the multi-step Single Normal Equation Simulation (SNESIM) algorithm of dyke structures in the Sungun Porphyry-Cu system, NW Iran. In order to perform a multi-step SNESIM algorithm, the multi-criteria decision-making and MPS approaches are used in a combined form. To this end, two TIs are considered, one for simulating dyke structures in the shallow depth, and two for simulating dyke structures in a deeper depth. In the first step, a TI is produced using geological map, which has been mined out during the previous exploration operations. After producing TI, the 35 realizations are simulated for the shallow depth of deposit in the area under study. To select the best realization (as a TI for the next step) of the simulation results, several statistical criteria are used and the results obtained are compared. To this end, a hybrid multi-criteria decision-making is designed on the basis of a group of statistical criteria. In the next step, the dyke structures in the deeper depth are also simulated by the new TI.

1. Introduction

There have been several studies dedicated to the modeling of different geological scenarios using various developed geostatistical methods [e.g. 1]. The conventional two-point geostatistics methods based on the variogram models have been employed to spatially interpolate the data [e.g. 2, 3], and they are now popular in different fields including mining, geology, and petroleum [4]. The critical issue in modeling geological structures is arising from the presence of heterogeneities and discontinuities in geological units like a swarm of dykes. The variogram-based techniques cannot

reproduce those non-linear continuities, and subsequently, they have a lack of accuracy in the reconstruction of a plausible geological model [e.g. 5]. As a solver in tackling such issues in the geological studies, the multiple-point geostatistics (MPS) has been proposed, where a training image (TI) prior to the geological/geophysical information is incorporated in the interpolation techniques [e.g. 6].

Various MPS techniques such as those of Tran (1994) [7] and Roberts (1998) [8] have been employed to improve the applicability of

✉ Corresponding author: o.asghari@ut.ac.ir (O. Asghari).

geostatistical modeling. Strebelle (2000) [9] has proposed the Single Normal Equation Simulation (SNESIM) algorithm, and later Caers (2001) [10] has used an invaluable tool to extract the features of patterns by combining the neural networks and MPS. Journel (2002) [11] has proposed the stationary relationship and information fusion to improve the simulation results. Note that an updated relationship has been introduced by Zhang and Journel (2002) to control the target function [12]. Arpat and Caers (2004) [13] have developed the Simulation Patch-based (SIMPAT) algorithm and its modified version [14]. The SNESIM algorithm, proposed by Strebelle (2002) [15], has been coded by Remy *et al.* (2007) [16] in the SGeMS open-source software. Zhang (2006) [17] has introduced the Filter-based Simulation (FILTERSIM) algorithm, later coded by Wu *et al.* (2007) [18] in SGeMS. Mariethoz *et al.* (2010) [19] have proposed the Direct Sampling (DS) algorithm as a novel and strong algorithm in MPS. Tahmasebi *et al.* (2012) [20] have proposed a new algorithm (CCSIM) for both the unconditional and conditional simulations with a raster path. Many research papers on the pattern-based approach have also published [21, 22]. Tahmasebi *et al.* (2014) [23] have developed and improved the CPU performance of the CCSIM algorithm in term of simulating categorical variables. Moura *et al.* (2017) [24] have proposed the LSHSIM method as a new method that generates realizations faster than the MS-CCSIM method [23]. Bavand Savadkoobi *et al.* (2019) [25] have used an effective combination of CCF and discrete wavelet transform (DWT) to improve the simulation results.

The key advantage of the MPS method, rather than the variogram model (two-point geostatistics), is the incorporation of a training image (TI) [26], where such a space underlies the total patterns and structures of the sought region [27]. The primary idea of TI has been presented based on the geological data [28]. In order to obtain TI, different methods such as the object-based simulation algorithm have been presented. If the geological model considers the repeatability of the geological phenomena, it can be assumed as an image. Novel methods with ability of importing a higher order statistics in simulation process utilize such images [29].

The ultimate motive of this research work was to run a multi-step SNESIM MPS method. In the first step, TI was prepared based on the geological setting, and then the dykes of shallow regions were simulated based on the best realization. It is

expected that the resulting simulated model is in close consistency with the real environment. Note that the optimum selection of the simulated geological model was casted in a multiple criteria decision-making (MCDM) problem, whilst the established statistical criteria could appropriately pick up the optimum geological model [an example of the statistical criteria can be found in 30-33]. The VIKOR method as the well-known MCDM approach [34, 35] was used to prioritize all realizations of geological models, leading to an optimal selection of the searched target. Since all the statistical criteria do not have an equal importance, we applied the Best-Worst Method (BWM), originally proposed by Rezaie (2015) [36] as an extension to the Analytic Hierarchy Process (AHP) to assign weight to each criterion before running the VIKOR method. The optimum realization was passed through the second step, where deeper portions of dykes were simulated successfully (Figure 1).

The major purpose of this research work was to model dykes as important mineralization control factors in the Sungun porphyry copper deposit. For this aim, the SNESIM algorithm was used as a strong MPS algorithm. The choice of a TI and its representativeness was a challenging issue subject to ongoing developments. In order to increase the accuracy of TI, the SNESIM algorithm was utilized with a staged algorithm. To this end, in the first step, the geological map and information were used to produce a TI for simulating the dyke structures in the shallow depth. Then the SNESIM method was used for reproducing the complex patterns of dykes in the shallow depth of the deposit. In the second step, the best realization was selected using the proposed hybrid MCDM method, which benefited from a mixture of the VIKOR, AHP, and BWM methods. The best realization was used as TI to reproduce 35 realizations over a deeper depth within the region of interest. Finally, several statistical criteria in the realizations were compared with those in TI (Figure 1).

2. Methodology

The following sub-sections describe concisely the MPS algorithm, AHP-BMW weighting approach, and VIKOR methodology, respectively.

2.1. SNESIM algorithm

The SNESIM algorithm, as introduced by Strebelle (2000) [9], solves the problem of two-point geostatistics by keeping the flexibility of the pixel-based techniques [26], where the probability functions are extracted from a TI. For the sake of

being as a pixel-based technique for simulation of complex geological phenomena, it outperforms the reproduced conditional data by scanning each considered pattern in input TI [26 and 37]. In

addition, the number of iterations is controlled by the probability rules to estimate a variable value at the desired simulated point [26 and 38].

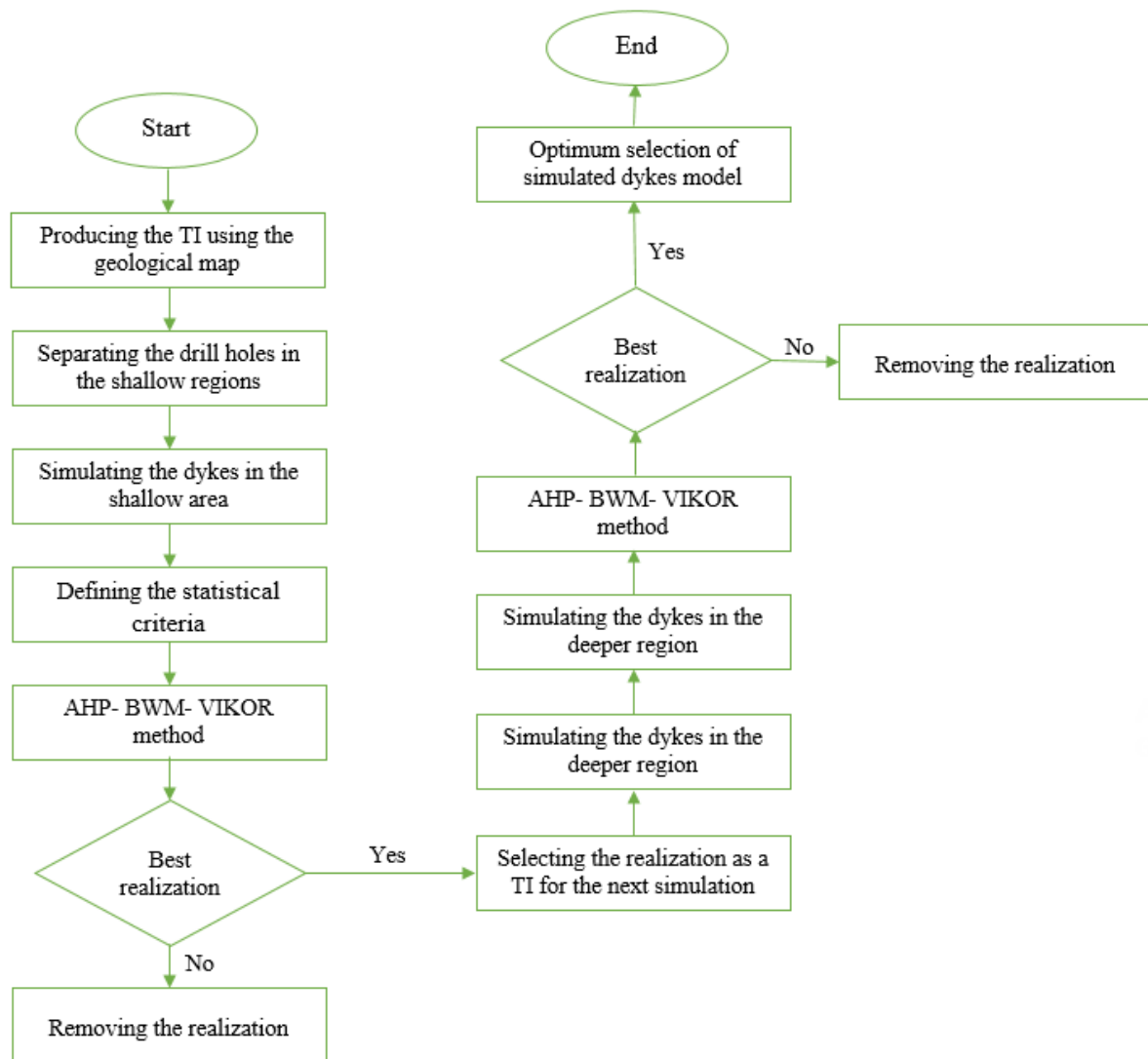


Figure 1. A flowchart illustrating the procedure according to the main purpose of this work.

In a sequential simulation approach, obtaining the cumulative probability density function (CPDF) plays an important role [26 and 39]. The point that should be noted is that CPDF of variogram-based geostatistics is obtained by the relationship between two points at each moment, whereas it is derived from the relationship between n points at a moment in MPS [15].

A_k , as a binary indicator variable of an occurrence for state s_k at location u , is defined by the following equation [15, 26, and 38]:

$$A_k = \begin{cases} 1 & \text{if } S(u) = s_k \\ 0 & \text{if not} \end{cases} \quad (1)$$

where D is denoted as a binary random variable connected to the occurrence of state d_n , which is formed with n conditional data [15, 26, and 38] such that:

$$A_k = \begin{cases} 1 & \text{if } S(u_a) = s_{k_a}, \forall a = 1, \dots, n \\ 0 & \text{if not} \end{cases} \quad (2)$$

The main purpose is to calculate the conditional probability value of D occurrence (s_k at location u), assuming that the event d_n happens in a D proximity. The conditional probability value is obtained through ordinary kriging (with $n + 1$ order statistics) in association with A_k and event D [26]:

$$\begin{aligned}
 Prob\{A_k = 1|D = 1\} \\
 = E\{A_k\} + \lambda[1 - E(D)]
 \end{aligned}
 \tag{3}$$

where $D = 1$ represents the occurrence of D , and $E\{D\} = Prob\{D = 1\}$ denotes the probability value of the event occurrence. Therefore, the weight value (λ) can be calculated as [15]:

$$\lambda Var\{D\} = Cov\{A_k, D\}
 \tag{4}$$

Where:

$$Cov\{A_k, D\} = E\{A_k, D\} - E\{A_k\}E\{D\}
 \tag{5}$$

Equation (4) can be re-written as [15]:

$$\lambda = \frac{E\{A_k, D\} - E\{A_k\}E\{D\}}{E\{D\}(1 - E\{D\})}
 \tag{6}$$

So:

$$\begin{aligned}
 Prob\{A_k = 1|D = 1\} &= E\{A_k\} + \frac{E\{A_k, D\} - E\{A_k\}E\{D\}}{E\{D\}(1 - E\{D\})} \\
 &= \frac{E\{A_k, D\}}{E\{D\}} = \frac{Prob\{A_k = 1|D = 1\}}{Prob\{D = 1\}}
 \end{aligned}
 \tag{7}$$

According to Equation (7), it is a Bayesian relation. TI is scanned in the later stage. The numerator is obtained by counting the number of iterations of events in TI, and the denominator is associated with a central cell value $S(u)$ equal to s_k (c_k and c) [15]. Finally, it is expected that the deduction value is similar to that of the target function of TI. Thus we have Equation (8).

$$\begin{aligned}
 p(u; s_k|n) &= Prob\{A_k = 1|D = 1\} \\
 &= Prob\{S(u) = s_k|n\} \\
 &\cong \frac{c_k(d_n)}{c(d_n)}
 \end{aligned}
 \tag{8}$$

2.2. AHP-BWM approach

The AHP method, proposed by Saaty (1977) [40], is a strong technique by capability of ranking several alternatives in a MCDM problem. One of the major features of this method is its flexibility for doing sensitivity analysis on the criteria and sub-criteria [41]. In addition, it is on the basis of constructing pairwise comparison matrices (PCMs) [42]. However, the main shortcoming is pertaining to the need for constructing several PCMs, leading to a huge number of pairwise comparisons. In order to tackle such a deficiency, Rezaie (2015) [36] has proposed BWM, in which the best and worst criteria are first chosen before estimating the weights of a number of criteria/factors. Then two pairwise comparison vectors (among the best/worst criteria and other criteria) are performed. The final stage of BWM is to formulate and solve a max-min problem for calculating the weights of different criteria [26 and 43-44]. Not only the BWM method reduces the

applied information (PCMs) but also this approach produces the results more valid than the other MCDM approaches [45].

Here, a hybrid AHP-BWM method is implemented by depicting the decision problem as a linear hierarchy based upon the AHP method. Then the weights of different factors in different levels of this hierarchy are determined via BWM. The following steps are required for running the hybrid AHP-BWM method [36 and 43-47]:

Step 1. Determining a linear hierarchy structure of the decision problem (designing a decision tree).

Step 2. Defining the best and worst criteria at each level.

Step 3. At each level of the hierarchy, constructing the first pairwise comparison vector as the preference degrees of the best criterion over all the other criteria. The elements of the pairwise comparison vector must be scaled at an interval from 1 to 9. This best-to-others vector can be written as:

$$A_B = (a_{B1}, a_{B2}, \dots, a_{Bn}),$$

where a_{Bn} represents the preference degree of the best criterion (B) than the criterion j , and a_{BB} is equal to one.

Step 4. At each level of the hierarchy, constructing the second pairwise comparison vector as the preference degrees of all criteria over the worst criterion. The elements of the pairwise comparison vector must be at a similar scale. This others-to-worst vector can be written as:

$$A_W = (a_{1W}, a_{2W}, \dots, a_{nW})^T,$$

where a_{jW} represents the preference degree of the criterion j than the worst criterion (W), and a_{WW} is equal to one.

Step 5. Calculating the optimal weights includes $(W_1^*, W_2^*, \dots, W_n^*)$. The pairs $\frac{w_B}{w_j} = a_{Bj}$ and $\frac{w_j}{w_w} = a_{jw}$ are formed for determination of the optimal weights. After this stage, in order to satisfy the explained conditions for each j , the maximum absolute differences $\left| \frac{w_B}{w_j} - a_{Bj} \right|$ and $\left| \frac{w_j}{w_w} - a_{jw} \right|$ should be minimized for each j . Thus the optimal weights can be obtained by reviewing the following non-linear programming model:

$$\min \max_j \left\{ \left| \frac{w_B}{w_j} - a_{Bj} \right|, \left| \frac{w_j}{w_w} - a_{jw} \right| \right\}$$

$$\begin{aligned}
 & \text{s.t.} \\
 & \sum_j w_j = 1 \\
 & w_j \geq 0, \text{ for all } j
 \end{aligned} \tag{9}$$

Also the non-linear model (Equation 9) is changed to a linear model, as follows:

$$\begin{aligned}
 & \min \xi \\
 & \text{s.t.} \\
 & |w_B - a_{Bj}w_j| \leq \xi, \text{ for all } j \\
 & |w_j - a_{jw}w_w| \leq \xi, \text{ for all } j \\
 & \sum_j w_j = 1 \\
 & w_j \geq 0, \text{ for all } j
 \end{aligned} \tag{10}$$

The optimal weights and ξ^* values are obtained by solving the above model.

Step 6. Calculating the consistency ratio (CR) by means of the ξ^* value and consistency index (CI). It is clear that a higher value of ξ^* represents a higher value of CR since $a_{Bj} \times a_{jw} = a_{BW}$ and $a_{BW} \in \{1, 2, \dots, 9\}$, the maximum value for ξ can be calculated. According to CI in Table 1 and Equation (11), CR can be inferred by:

$$CR = \frac{\xi^*}{\text{Consistency Index}} \tag{11}$$

Based on the CR value, the values equal to or lesser than 0.1 represent a reliable result.

Table 1. CI table for using the BWM method.

a_{BW}	1	2	3	4	5	6	7	8	9
$CI (\max \xi)$	0.00	0.44	1.00	1.63	2.30	3.00	3.73	4.47	5.23

2.3. VIKOR methodology

Opricovic and Tzeng (2004) [34] have introduced the first version of the VIKOR technique as a powerful tool to select the best alternative in MCDM problems. According to its formulation, different alternatives under various criteria and sub-criteria are compared by an ideal solution on the basis of a distance measure [48-51]. As a prominent approach, it can be utilized in compromise ranking problems [52]. An integrated function, so-called L_P -metric, is used to generate the compromise ranking [35]. The alternatives and criteria are defined as A_1, \dots, A_n and C_1, \dots, C_m , respectively, where a_{ij} represents the score of the i th alternative based on the j th criterion function. Based on the L_P -metric, expansion of the VIKOR method can be defined as:

$$L_{p,j} = \left\{ \sum_{i=1}^m [w_i(f_i^+ - a_{ij}) / (f_i^+ - f_i^-)]^p \right\}^{\frac{1}{p}} \tag{12}$$

where $1 \leq P \leq \infty$ and $i = 1, \dots, m$.
 where $1 \leq P \leq \infty$ and $i = 1, \dots, m$.

In the conventional formulation, $L_{ij} = S_j = \sum_{i=1}^m [w_i(f_i^+ - a_{ij}) / (f_i^+ - f_i^-)]$ and $L_{\infty j} = R_j = \max_i \left\{ \frac{w_i(f_i^+ - a_{ij})}{f_i^+ - f_i^-} \right\}$ are subsequently calculated [29], where w_i is the weight of the j th criterion. As mentioned, this weight was extracted by implementing the AHP-BMW in this work. L_{ij} provides the information for maximum group utility, while $L_{\infty j}$ is the information of minimum

opposite individual effect. The VIKOR algorithm can be summarized in the following steps [35]:

Step 1. Calculating the positive ideal solution (f_i^+) and negative ideal solution (f_i^-) alternative values for each criterion ($i = 1, \dots, m$) by the following equations:

If it is a benefit mode problem

$$f_i^+ = \max_j \{a_{ij}\}, \quad f_i^- = \min_j \{a_{ij}\} \tag{13}$$

If it is a cost mode problem.

$$f_i^+ = \min_j \{a_{ij}\}, \quad f_i^- = \max_j \{a_{ij}\}$$

Step 2. Calculating the S_j and R_j values by the aforementioned equations ($j = 1, 2, \dots, J$).

Step 3. Determining the Q_j ($j = 1, 2, \dots, J$) value:

$$Q_j = \left(\frac{S_j - S^+}{S^- - S^+} \right) + (1 - \gamma) \left(\frac{R_j - R^+}{R^- - R^+} \right) \tag{14}$$

The parameters in Equation (14) are equal to $S^+ = \min_j \{S_j\}$, $S^- = \max_j \{S_j\}$, $R^+ = \min_j \{R_j\}$, $R^- = \max_j \{R_j\}$, and γ represents the weight of the strategy of “the majority of criteria” (or “the maximum group utility”). γ is generally assumed equal to 0.5. Also Q_j denotes the weight of VIKOR for the j th alternative.

Step 4. Based on the S_j , R_j , and Q_j values, alternatives are sorted in a decreasing order.

Step 5. Selecting the best alternative, the best compromise solution can be selected by satisfying these two conditions:

1. Acceptable advantage:

$$Q(A^{(2)}) - Q(A^{(1)}) \geq DQ \quad (15)$$

where:

$$DQ = \frac{1}{n-1} \quad (DQ = 0.25 \text{ if } n \leq 4)$$

and based on the Q value, $A^{(1)}$ and $A^{(2)}$ are the alternatives with the first and second positions, respectively. In addition, n denotes the number of the available alternatives.

2. Acceptable stability in decision-making. According to this condition, the alternative $A^{(1)}$ should be located in the best rank at the S , R , and Q criteria. If the first condition is not satisfied and $Q(A^{(N)}) - Q(A^{(1)}) < DQ$, then $A^{(1)}, A^{(2)}, \dots, A^{(n)}$ are selected as the same compromise solution. If the second condition is not satisfied, the alternatives $A^{(1)}$ and $A^{(2)}$ are selected as the same compromise solution.

3. Case study

The region of interest is located in the NW Iran at the East-Azerbaijan Province (Figure 2). The Sungun porphyry copper system occurs over the Sahand-Bazman volcanic and plutonic belt (or the Urumia-Dokhtar Magmatic Assemblages, UDMA). The field survey and petrology studies identify several stocks in the Sungun system, which causes a hydrothermal alteration system [53]. Diorite/granodiorite to quartz monzonite rocks have dominated this copper system [54, 55]. The tonnage of the Sungun porphyry deposit is more than 500 Mt sulfide reserve at an average grade of 0.76% copper and 0.01% molybdenum. The mineralized portions of the Sungun deposit occurred mostly in stock units with depletion in dyke intrusions [53]. The important stocks in association with porphyry copper mineralization include porphyry stock I (quartz monzonite) and II (quartz monzonite to granodiorite/diorite) [56]. Note that there are four types of dykes in the region, which typically comprise quartz monzonite to granodiorite/diorite [56]. These dykes have cut the Cu mineralization at several phases leading to sectors with a depleted content of Cu ore.

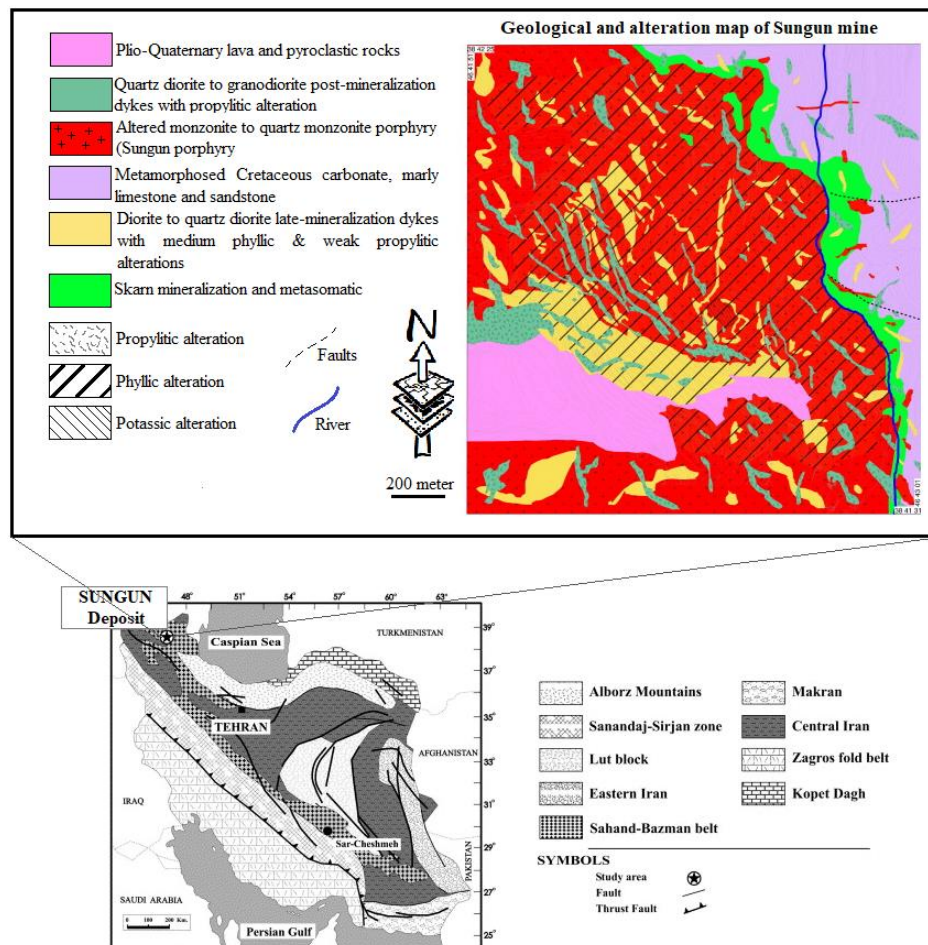


Figure 2. Location and geology map of the Sungun porphyry copper deposit.

The general trend of dykes is NW-SE (parallel to the UDMA tectonic unit), and their thickness changes from a few centimeters to several tens of meters (Figure 3). Among different dyke patterns in Sungun, DK1 has the most frequencies, where its constituents change from quartz diorite to quartz

monzonite. Based on the isotope, mineralogy, and alteration studies, the DK1 unit is divided into the three types of DK1a, DK1b, and DK1c. Roughly speaking, the average grade of copper is very low and below the economic cut-off value in the DK1.

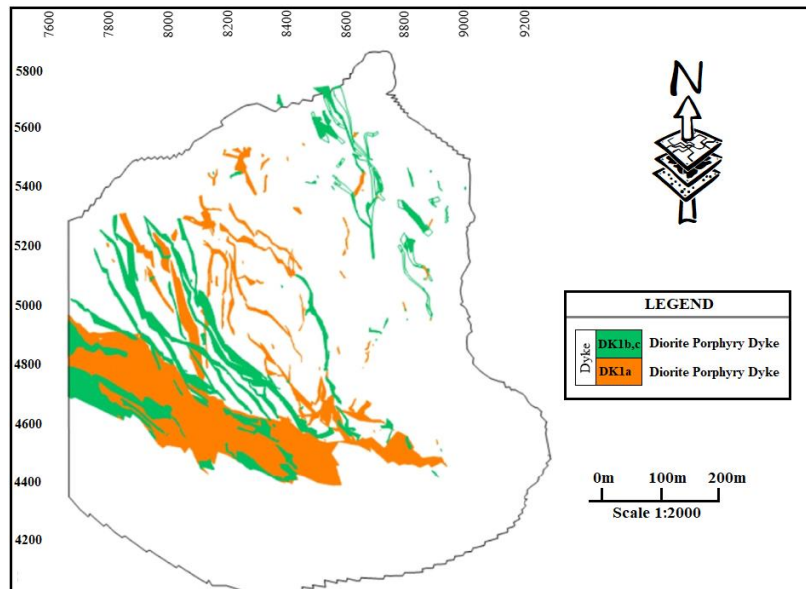


Figure 3. DK1 map of the Sungun porphyry copper deposit.

The Sungun deposit was sampled by the vertical, horizontal, and steep drill holes in the detailed exploration phase. The drilled holes were designed in a regular network at an interval of 100 m. All the collected and analyzed samples was 41520 for grade and geological features. In order to satisfy the stationarity conditions, those portions of the Sungun system obeying such conditions were simulated (Figure 4). According to Figure 3, DK1a and DK1b have dominated the studied region. Therefore, they were used for simulation of the dykes. To sequentially simulate the dykes of shallow area, the DK1 map of the Sungun porphyry copper deposit (prepared from surface geological map) can be used as a TI to run the first step of MPS. After extracting DK1a and DK1b, TI was projected on the topography map (Figure 5). The proportion and variance of TI and actual data need to be compared as well to check TI representativeness. Table 2 shows that the main statistics of TI is similar to that obtained with the hard data.

Table 2. Statistical parameters of TI and hard data.

	Proportion	Variance
TI	0.338	0.224
Hard data	0.321	0.221

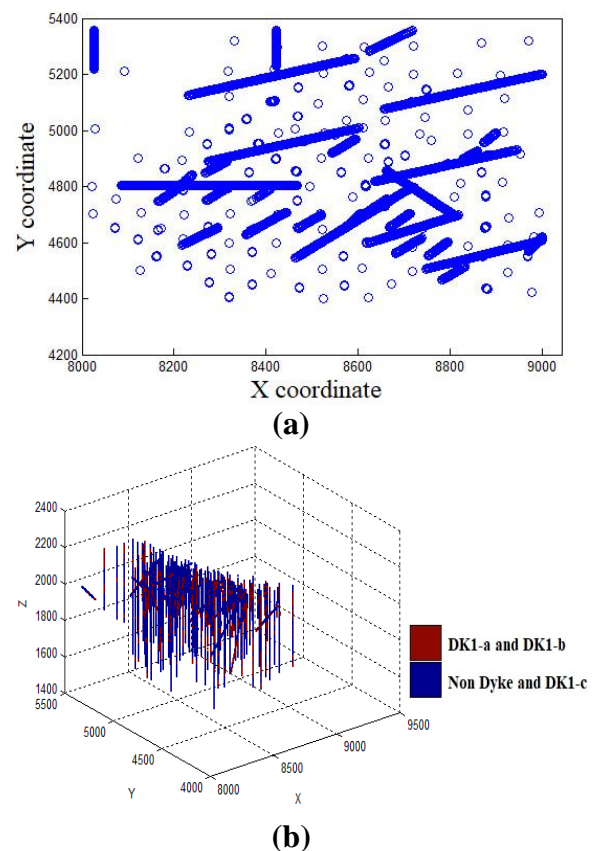


Figure 4. (a) Top view and (b) 3D view of drilled holes in the Sungun porphyry copper deposit for those regions with stationarity conditions.

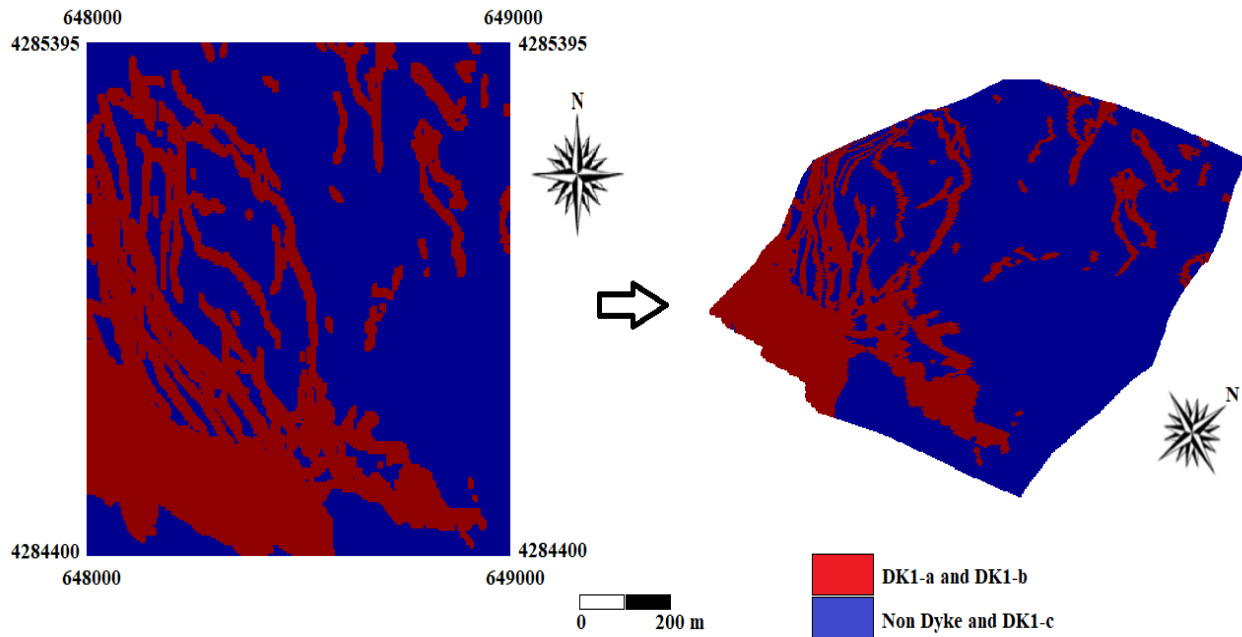


Figure 5. Training image extracted from the DK1 map for modelling the dykes of shallow region.

4. Optimum selection of simulated dyke model

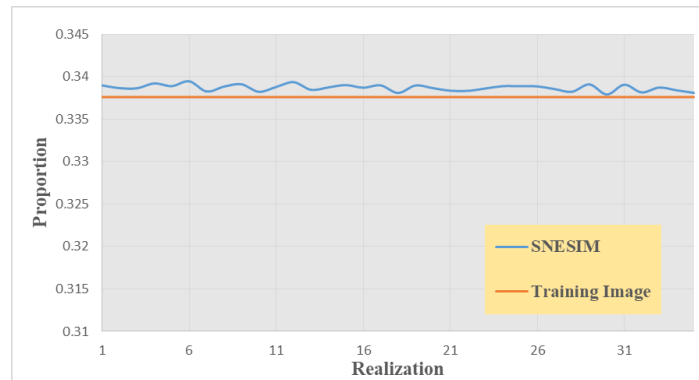
The primary input of the SNESIM algorithm is the simulation grid. A block model of the desired area was produced with the grid size of $10 \times 10 \times 10$ m. At the first step, TI derived from the DK1 map was inserted as an important input. The search radius was fixed with a constant value for all directions. In this case, it can be clearly seen that the SNESIM algorithm is capable of identifying the conditional data patterns [57]. In this work, the continuity of the dykes was reduced by means of the anisotropy search pattern. Based on the trial-and-error method, the range of the search pattern was assumed to be 150 m. The number of data in the search pattern is a main factor of the SNESIM algorithm. In addition to the importance of this factor in controlling the reproduced patterns, this factor has the highest impact on the computational efficiency of the algorithm. Taking the runtime of the algorithm and reproducing the large-scale structures into account, the number of data in the search pattern was about 140. The simulation could be performed by the conditional or non-conditional data. Because of the high reality of modeling in the conditional simulation, this type of simulation was used here for the hard data collected by drilling. According to the research work by Liu (2006) [57], the simulated facies may not satisfy the directional parameters and stationarity conditions, and

therefore, zoning trick can tackle such a problem in this work.

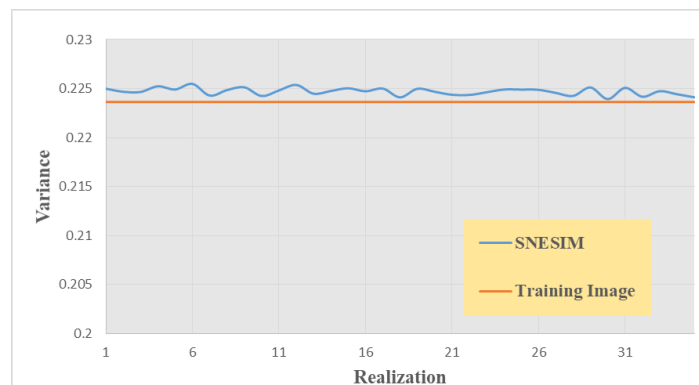
4.1. Shallow region simulation

Taking TI of the DK1 map, and the lithology data from the drilled holes in the shallow regions of the Sungun into consideration, simulation of DK1a and DK1b was carried out through running the SNESIM algorithm. After the first step, the optimum simulated realization was searched for generating a TI input for implementing simulation at deeper portions in the second step. Various statistical criteria such as single-point statistics, two-point statistics, multiple-point statistics, connectivity reproduction, and high order covariance reproduction (Cumulants) are incorporated in a MCDM problem to choose the best realization of simulation.

The single-point characteristics of different realizations for selection of the best simulated output were used as the proportion and variance criteria, where TI was used to compare all the simulation results. The proportion and variance obtained from all realizations are plotted in Figures. 6a and 6b, respectively. They represent a little difference between the single-point statistical parameters of the simulation in all realizations and those derived from TI, enhancing the advantage of the SNESIM algorithm in considering the servosystem factor.



(a)



(b)

Figure 6. Graphical comparison of the single-point statistics parameters of the TI and SNESIM realizations (a) proportion, and (b) variance.

When there are differences between the proportion of the target function for hard data and the TI map, the servosystem factor must be used for the SNESIM algorithm [15]. The difference between the proportion of the target function and the simulation can be reduced by means of the servosystem factor. This correction must be done by the servosystem factor at each step of the simulation process. Let us assume that $P(A)$ and $P_c(A)$ are the target function of hard data and moment target function of TI, respectively. The correction function is represented by the following equation:

$$p^{new}(A|B) = P(A|B) + \mu(P(A) - P_c(A)) \quad (16)$$

where μ can be calculated as:

$$\mu = \frac{\lambda}{1 - \lambda}, \quad \lambda \in [0,1] \quad (17)$$

It is clear that a higher value of λ coincides with a higher correction. Figure 7 indicates the sensitivity of the target function versus the servosystem factor (λ), meanwhile the final correction value is equal to 0.87.

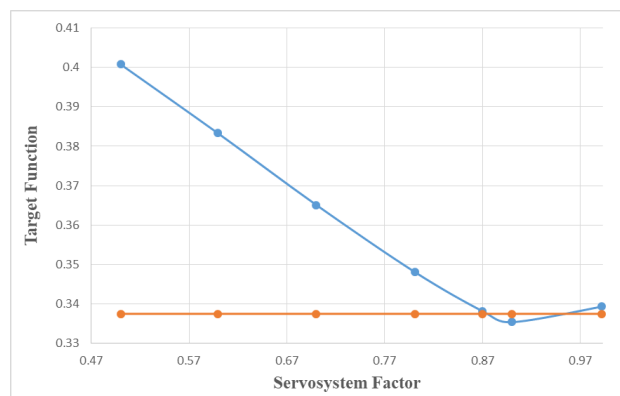


Figure 7. The linear variation of the target function versus the servosystem factor.

Based on the proportion and variance of TI, a quantitative comparison of the single-point statistics parameters of the SNESIM realizations was done by the following equations:

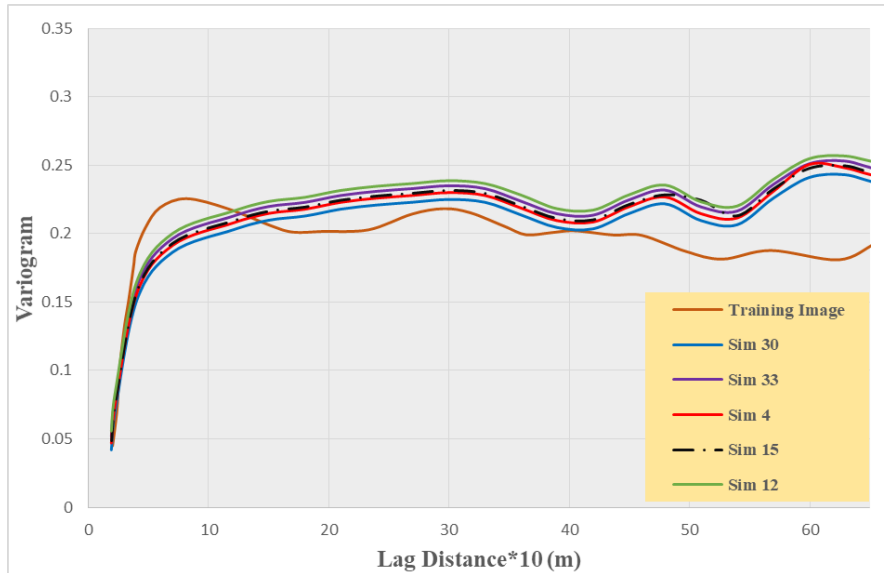
$$\Delta\mu = \mu_R - \mu_{TI} \tag{18}$$

$$\Delta\sigma = \sigma_R - \sigma_{TI} \tag{19}$$

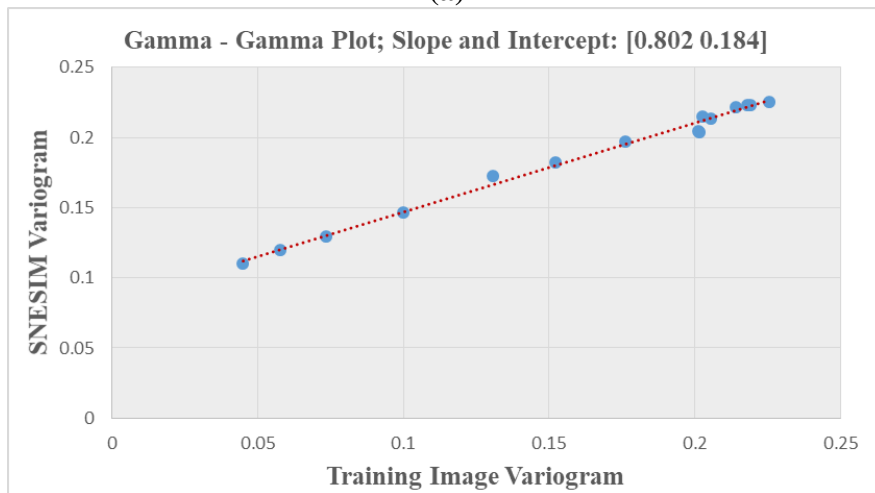
where μ_R and σ_R are the proportion and variance of the realizations, respectively. Also μ_{TI} and σ_{TI} are the proportion and variance of TI, respectively. It is clear that a lower value of $\Delta\mu$ and $\Delta\sigma$ represents a more appropriate realization.

Since variogram is a tool for checking the two-point statistics, we compared the omni-directional variogram model of TI and each realization as a

criterion in selection of the best simulated result. The omni-directional variogram obtained from the five realizations (as representatives of all) and TI are all shown in Figure 8a. This process must be plotted for all realizations. In order to a quantitatively compare the variogram models, the Gamma–Gamma plots were used [17], where the correlation coefficients between TI and all realizations are obtained by the Gamma–Gamma plots. Note that a higher correlation coefficient corresponds to a more suitable realization. The Gamma–Gamma plot of the realization #30 versus TI is shown in Figure 8b. Such plots must be calculated for all realizations. Based on the highest slope of the linear curve fitted between TI and realization #30 (0.802), this realization generated the most suitable one.



(a)



(b)

Figure 8. Omni-directional variogram of five realizations and TI for shallow region (a) and Gamma-Gamma plot of the realization #30 versus TI (b).

The TI and SNESIM realizations were compared through multi-point statistics using the Peredo and Ortiz method (2011) [58], where all realization must be scanned after selecting a search pattern in 1D, 2D or 3D. Then the clustering of the extracted patterns is done to locate all similar patterns in different clusters. The frequency of similar patterns is saved as the important factor. The reproduced patterns of the SNESIM realizations and TI were compared through plotting the frequency chart of patterns on the SNESIM realizations and TI. Assuming a 5×5 network due to the original TI, the obtained result from the realization #30 versus TI was shown in Figure 9. Based on the fitted linear curve for the first and third quarter, the optimum realization can be introduced via this criterion.

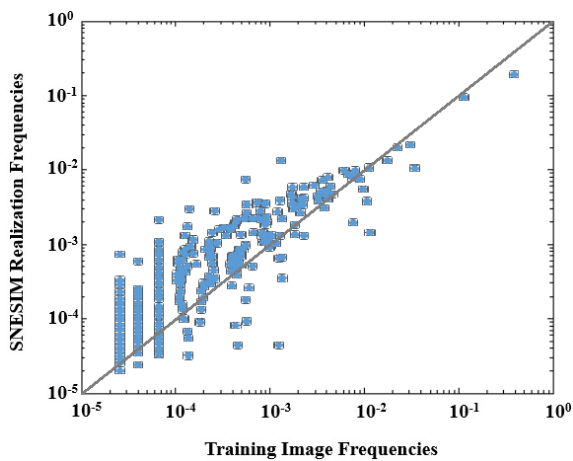


Figure 9. Frequency chart of reproduced patterns on the realization #30 and TI.

Since the main purpose of this work was to reproduce the dyke connectivity, this feature of the dykes can be a suitable criterion in the optimum selection of a realization among all the generated geological models. Generally speaking, n -point probability of connection in a particular direction is calculated by the following equation [59]:

$$E \left\{ \prod_{j=1}^n I[u + (j - 1)h; z] \right\} = \varphi(n) \quad (20)$$

It is clear that increasing the number of points causes the reduction of the probability value of connectivity reproduction. For one point, the probability value is equal to the proportion of the target function. The selected direction for calculation of probability of connection is 135° , which is parallel to the trend of the dykes. The probability value of connectivity reproduction obtained from the five realizations (as representatives) and TI are plotted in Figure 10. Considering the probability value of connectivity reproduction of TI, quantitative comparison of the probability value of connectivity reproduction of the SNESIM realizations is calculated by:

$$H = \sum_{i=1}^{16} \varphi_{realization_i} - \varphi_{Training Image_i} \quad (21)$$

where i denotes the number of points. A lower value of H corresponds to a more suitable realization.

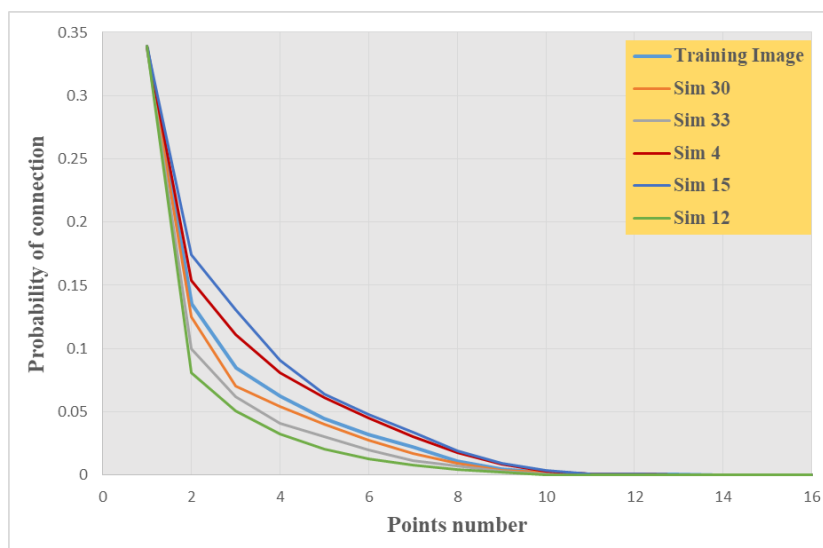


Figure 10. Probability value of connectivity reproduction of the SNESIM realizations and TI.

Cumulants were firstly introduced by Dimitrakopoulos *et al.* (2010) [60] for modeling of geological phenomena. De Iaco and Maggio (2011)

[61] did a comparison between the sequential indicator simulation (SIS) realizations and the SNESIM realizations by higher order Cumulants.

Let us assume that $(\Omega, \mathfrak{S}, P)$ and $(R^n, \beta(R^n))$ are a probability space and measurable space (in the probability space), respectively. Also assume that $Z(x)$ as a random field satisfies the stationarity conditions, and its mean is equal to zero in the R^n space. The r -order momentum of $Z_i = Z(x_i)$ is calculated by the following equation [60]:

$$Mom[Z_i^r] \Delta E\{Z_i^r\} = \frac{1}{j^r} \frac{d^r}{dw^r} [\phi(\omega)]_\omega = 0 \quad (22)$$

where $E\{\cdot\}$ represents the expectation operation and j^2 is equal to -1. $\phi(\omega)$ denotes the first characteristic function. The characteristic function can be written as [60]:

$$\phi(\omega) = E[e^{j\omega Z}] = \int_{-\infty}^{+\infty} e^{j\omega u} dF_Z(u) \quad (23)$$

The r -order Cumulants can be calculated through the r -order differential of the second characteristic function, which is equal to $\psi(\omega) = \ln(\phi(\omega))$. Thus it can be [60]:

$$Cum[Z_i, \dots, Z_i] = \frac{1}{j^r} \frac{d^r}{dw^r} [\psi(\omega)]_\omega = 0 \quad (24)$$

Let us assume that $E_{j_1, \dots, j_n} = E(X_1, \dots, X_n)$ and $C_{j_1, \dots, j_n} = Cum(X_1, \dots, X_n)$ are a n -order momentum and n -order Cumulant, respectively. Equation (25) represents a relationship between momentum and Cumulant [60].

$$m_{i_1, \dots, i_n} = \sum_{j_1=0}^{i_1} \dots \sum_{j_{n-1}=0}^{i_{n-1}} \sum_{j_n=0}^{i_n} \binom{i_1}{j_1} \dots \binom{i_{n-1}}{j_{n-1}} \binom{i_n}{j_n} \times C_{i_1-j_1, \dots, i_{n-1}-j_{n-1}, i_n-j_n} m_{j_1, \dots, j_n} \quad (25)$$

Also [55];

$$C_{i_1, \dots, i_n} = \sum_{j_1=0}^{i_1} \dots \sum_{j_{n-1}=0}^{i_{n-1}} \sum_{j_n=0}^{i_n} \binom{i_1}{j_1} \dots \binom{i_{n-1}}{j_{n-1}} \binom{i_n}{j_n} \times m_{i_1-j_1, \dots, i_{n-1}-j_{n-1}, i_n-j_n} C_{j_1, \dots, j_n} \quad (26)$$

Now, assume that Z_x is a variable with zero mean. The r -order momentum can be calculated as [60]:

$$Mom[Z(x), Z(x+h_1), \dots, Z(x+h_{r-1})] = E[Z(x)Z(x+h_1) \dots Z(x+h_{r-1})] \quad (27)$$

In this space, the momentum value is associated with the distance vectors (h_1, h_2, h_3) . Therefore, the r -order Cumulant can also be calculated as [60]:

$$C_r^Z[h_1, h_2, \dots, h_{r-1}] = Cum[Z(x)Z(x+h_1) \dots Z(x+h_{r-1})] \quad (28)$$

In order to calculate the Cumulant value, the distance vectors must be determined. Therefore, each spatial template can be defined using the following equation as [60]:

$$T_{n+1}^{h_1, h_2, \dots, h_n}(h_1, h_2, \dots, h_n, a_1, a_2 \dots a_n) = \{x, x+h_1, x+h_2, \dots, x+h_n\} \quad (29)$$

Finally, the 3-order Cumulant is computed [60]:

$$C^{T_3^{h_1, h_2}} = \frac{1}{N_{h_1, h_2}} \sum_{k=1}^{N_{h_1, h_2}} Z(x_k)Z(x_{k+h_1})Z(x_{k+h_2}), x_k: x_{k+h_1}: x_{k+h_2} \in T_3^{h_1, h_2} \quad (30)$$

Similarly, 4-order Cumulant is inferred as [60, 61]:

$$C^{T_4^{h_1, h_2, h_3}} = \frac{1}{N_{h_1, h_2, h_3}} \sum_{k=1}^{N_{h_1, h_2, h_3}} Z(x_k)Z(x_{k+h_1})Z(x_{k+h_2})Z(x_{k+h_3}) - \frac{1}{(N_{h_1, h_2, h_3})^2} \left[\left(\sum_{k=1}^{N_{h_1, h_2, h_3}} Z(x_k)Z(x_{k+h_1}) \right) \left(\sum_{k=1}^{N_{h_1, h_2, h_3}} Z(x_{k+h_2})Z(x_{k+h_3}) \right) \right] - \frac{1}{(N_{h_1, h_2, h_3})^2} \left[\left(\sum_{k=1}^{N_{h_1, h_2, h_3}} Z(x_k)Z(x_{k+h_2}) \right) \left(\sum_{k=1}^{N_{h_1, h_2, h_3}} Z(x_{k+h_1})Z(x_{k+h_3}) \right) \right] - \frac{1}{(N_{h_1, h_2, h_3})^2} \left[\left(\sum_{k=1}^{N_{h_1, h_2, h_3}} Z(x_k)Z(x_{k+h_3}) \right) \left(\sum_{k=1}^{N_{h_1, h_2, h_3}} Z(x_{k+h_1})Z(x_{k+h_2}) \right) \right] \quad (31)$$

In this work, Cumulants were used as a criterion to select the best realization. According to the spatial structure of the dykes (Figure 11 and Table 3), the calculation of Cumulants is divided into two groups (Figure 12):

1. The 3-order Cumulant in the three directions: {315, 45}, {135, 135}, and {315, 135}.

2. The 4-order Cumulant in the two directions: {315, 135, 45}, and {135, 135, 135}.

We compared two Cumulants comprising the former from TI (as a criterion) and the later from each realization. For a quantitative comparison of the Cumulants of TI and the SNESIM realizations, the mean squared error (MSE) and correlation methods were used for each realization (Table 4).

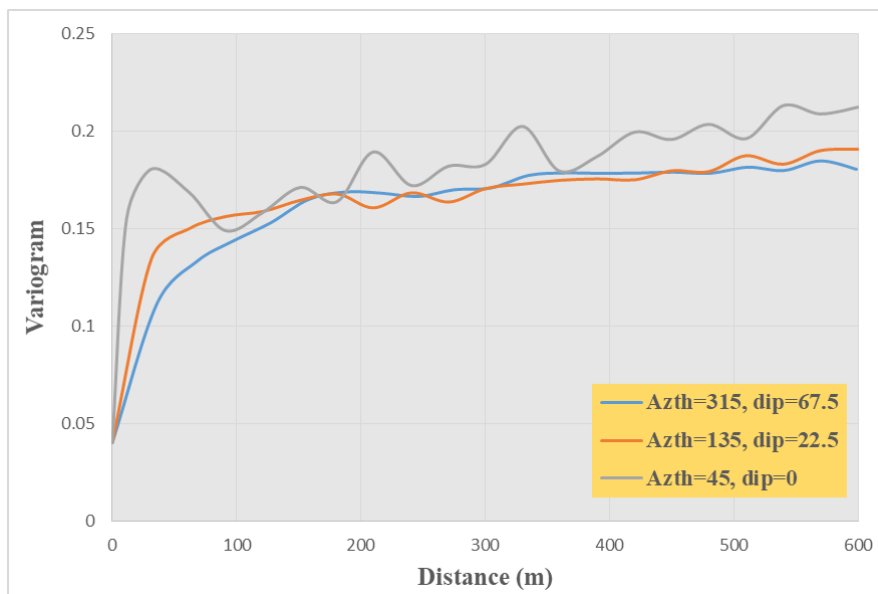


Figure 11. Experimental variogram of hard data in 3D.

Table 3. Characteristics of experimental variogram of hard data in 3D.

	Azimuth	Dip	Range (m)
1	315	67.5	180
2	135	22.5	78
3	45	0	54
Nugget effect	0.04	Sill	0.13

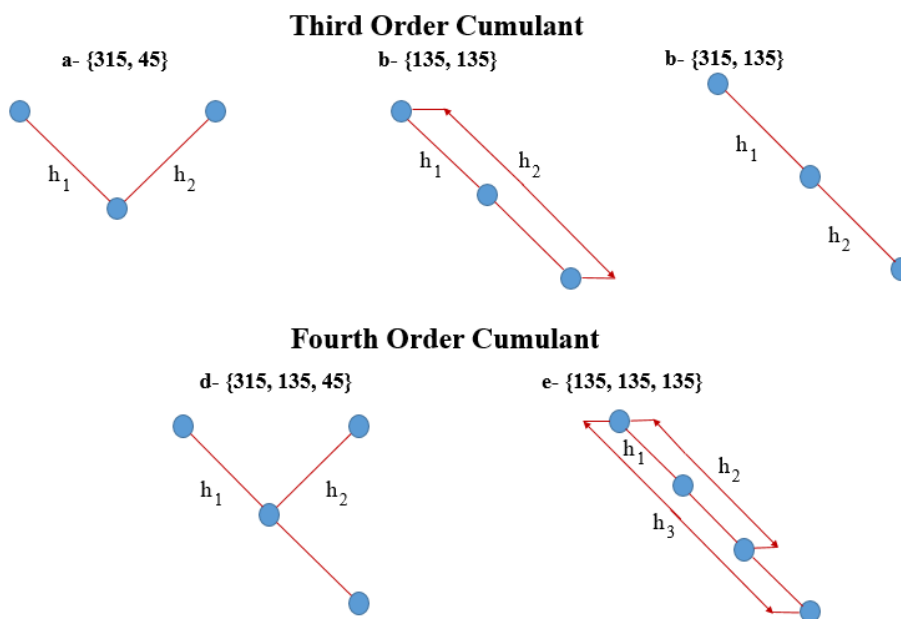


Figure 12. The considered patterns for calculation of Cumulants based on the spatial structure of the dykes.

Table 4. MSE and correlation results of Cumulants using considered patterns (for part of the realizations).

Considered pattern	Realization number	Mean squared error	Correlation
{315, 45}	30	127×10^{-7}	0.884
	33	122×10^{-7}	0.892
	4	174×10^{-7}	0.812
	15	191×10^{-7}	0.798
	12	184×10^{-7}	0.807
{135, 135}	30	101×10^{-7}	0.905
	33	124×10^{-7}	0.871
	4	201×10^{-7}	0.852
	15	182×10^{-7}	0.861
	12	214×10^{-7}	0.804
{315, 135}	30	175×10^{-7}	0.854
	33	192×10^{-7}	0.814
	4	214×10^{-7}	0.801
	15	222×10^{-7}	0.794
	12	241×10^{-7}	0.781
{315, 135, 45}	30	99×10^{-8}	0.942
	33	117×10^{-7}	0.898
	4	104×10^{-7}	0.903
	15	127×10^{-7}	0.891
	12	131×10^{-7}	0.884
{135, 135, 135}	30	109×10^{-7}	0.912
	33	116×10^{-7}	0.901
	4	193×10^{-7}	0.802
	15	142×10^{-7}	0.821
	12	125×10^{-7}	0.867

After checking the important criteria for the selection of the best realization, the BWM method was used to assign the criteria weight. The hierarchy structure of the main criteria and sub-criteria was designed in a decision tree shown in Figure 13. Based on the experts' judgment, the best and worst criteria were first determined, and then steps of the BWM method were followed. Finally,

solving a linear model (Equation 10) through the GAMS software, the ξ^* value and criteria weight at each part of hierarchy structure were calculated (Table 5). According to the consistency ratio, we concluded that the implemented linear model produced a consistent result.

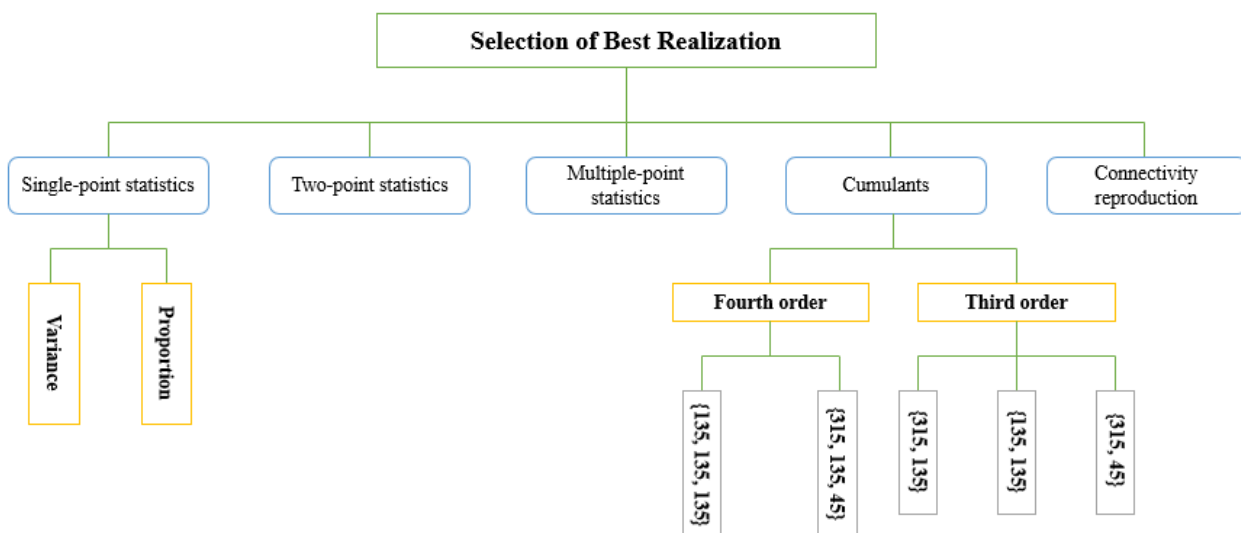


Figure 13. Hierarchy structure of the effective criteria for the selection of the best SNESIM realization.

Table 5. The optimal weight of each effective criterion from the BWM method.

Criteria	w_j	Sub-criteria	w'_j	Sub-criteria	w''_j	Final weight	
Single-point statistics	0.094	Proportion	0.500			0.047	
		Variance	0.500			0.047	
Two-point statistics	0.210						0.210
Multiple-point statistics	0.216						0.216
Connectivity	0.228						0.228
Cumulants	0.252	Third order	0.453			{315, 45}	0.294
				{135, 135}	0.412	0.047	
				{315, 135}	0.294	0.034	
		Fourth order	0.547	{315, 135, 45}	0.500	0.0685	
				{135, 135, 135}	0.500	0.0685	
ξ^*				0.134			
C.R.				0.027			

To rank 35 realizations obtained from the SNESIM algorithm, a decision matrix must be constructed for 35 alternatives and 16 criteria. The main purpose of this process is to select the best realization as a TI for simulation of dykes in the

deeper region (procedure shown in Figure 1). After making the decision matrix, this matrix must be normalized. In order to produce the homogeneous criteria (by positive nature), the linear normalization method must be used as [62, 63],

$$n_{ij} = \frac{a_{ij}}{\max_i \{a_{ij}\}}; i = 1, \dots, m, j = 1, \dots, n \quad \text{if it is a benefit mode problem}$$

$$n_{ij} = \frac{\frac{1}{a_{ij}}}{\max_i \left\{ \frac{1}{a_{ij}} \right\}} = \frac{\frac{1}{a_{ij}}}{\frac{1}{\min_i \left\{ \frac{1}{a_{ij}} \right\}}} = \frac{\min_i \left\{ \frac{1}{a_{ij}} \right\}}{\frac{1}{a_{ij}}} \quad \text{if it is a cost mode problem} \tag{32}$$

where a_{ij} represents the element value of alternative i in criterion j . Based on the steps of the VIKOR method, the values of normal matrix for each criterion are multiplied by criterion weight in order to calculate the weighted normal matrix. According to the application of the linear normalization method, the ideal solution of each criterion is equal to the maximum value in its

column. Finally, the $S, R,$ and Q values were calculated, and the best realization was selected based on the calculated values. The part of results obtained by the VIKOR method is shown in Table 6, while realization #30 was selected as the best one (Figure 14). Therefore, this realization was used as TI in the simulation of deeper portions in the Sungun porphyry-Cu deposit.

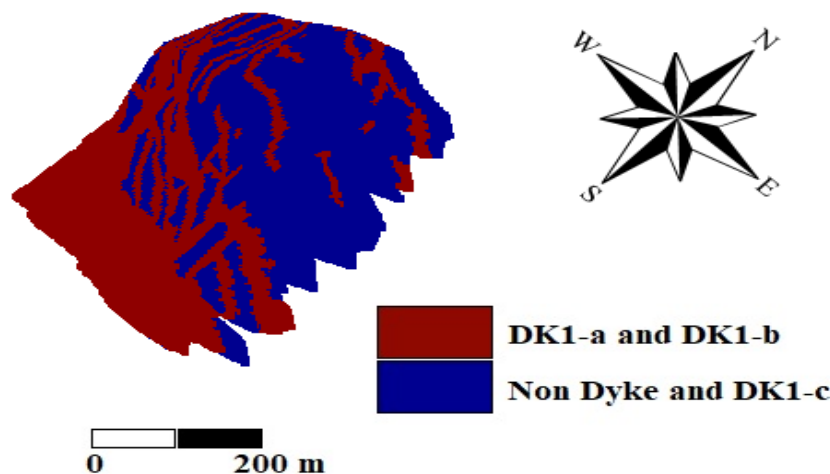


Figure 14. A 3D view of the best realization #30 by implementing the SNESIM algorithm in the shallow portions of the Sungun porphyry-Cu deposit.

Table 6. The final results obtained by the VIKOR method for shallow portions of the Sungun deposit.

Realization number	S	R	Q	Rating
30	0.088	0.418	0.293	1
33	0.033	0.541	0.299	2
4	0.073	0.506	0.322	3
15	0.299	0.172	0.388	4
8	0.384	0.086	0.432	5
5	0.006	0.893	0.450	6
11	0.389	0.143	0.467	7
1	0.089	0.811	0.496	8
10	0.488	0.016	0.505	9
2	0.060	0.933	0.528	10
26	0.330	0.463	0.570	11
25	0.270	0.597	0.575	12
7	0.314	0.540	0.592	13
6	0.379	0.729	0.758	14
19	0.312	0.957	0.804	15
28	0.321	0.950	0.810	16
13	0.740	0.111	0.819	17
21	0.710	0.208	0.837	18
34	0.381	0.982	0.889	19
23	0.828	0.080	0.894	20
14	0.746	0.295	0.920	21
17	0.666	0.478	0.929	22
18	0.527	0.764	0.931	23
12	0.524	0.774	0.932	24
22	0.430	0.989	0.944	25
24	0.597	0.652	0.947	26
29	0.634	0.599	0.957	27
3	0.669	0.949	1.175	28
16	0.847	0.609	1.186	29
35	0.742	0.857	1.203	30
32	0.815	0.730	1.215	31
9	0.960	0.446	1.221	32
27	0.766	0.911	1.256	33
20	0.838	0.936	1.345	34
31	0.910	0.867	1.385	35

4.2. Deep region simulation

According to the defined parameters for the simulation of the dykes in the shallow region (first step, Figure 1), the SNESIM realizations of the deeper region were conducted based on the optimum realization (TI) of the shallow region. Similar to the previous section, the criteria evaluation for selection of the best realization were investigated as well. They were generated for single-point statistics (Figures. 15a and 15b), two-point statistics (Figures. 15c and 15d), multiple-point statistics (Figure 15e), connectivity reproduction (Figure 15f), and high order covariance reproduction (Table 7).

Similar to the previous section, the realizations obtained from the SNESIM algorithm in the deep region were sorted based on Table 4 and decision matrix. The results obtained by the VIKOR method is shown in Table 8, where realization #22 is selected as the best one (Figure 16). The connectivity of dykes is reproduced using this hybrid method. Based on the result obtained by this method, the dykes of the Sungun system are generally located along the stretch of NW-SE trend

parallel to the UDMA structural zone in Iran. The DK1 map of the area under study proves that the general trend of dykes has happened in the NW-SE direction (Figure 3).

When applying the proposed approach and simulating the dyke structures, there is an interest to know about the accuracy and quality of the best simulation model. To this end, the single-point and two-point statistics of dyke in the best realization #22 are compared with those in the hard data. Table 9 shows that the proportion and variance of realization #22 are similar to those obtained with the hard data. Since variogram is a tool for checking the two-point statistics, the variogram models of the best realization #22 in the major, minor, vertical, and omni directions are compared with those in the hard data (Figure 17). It can be seen that the variogram parameters of realization #22 are close to hard data.

Table 9. Statistical parameters of TI and hard data.

	Proportion	Variance
Realization #22	0.339	0.225
Hard data	0.321	0.221

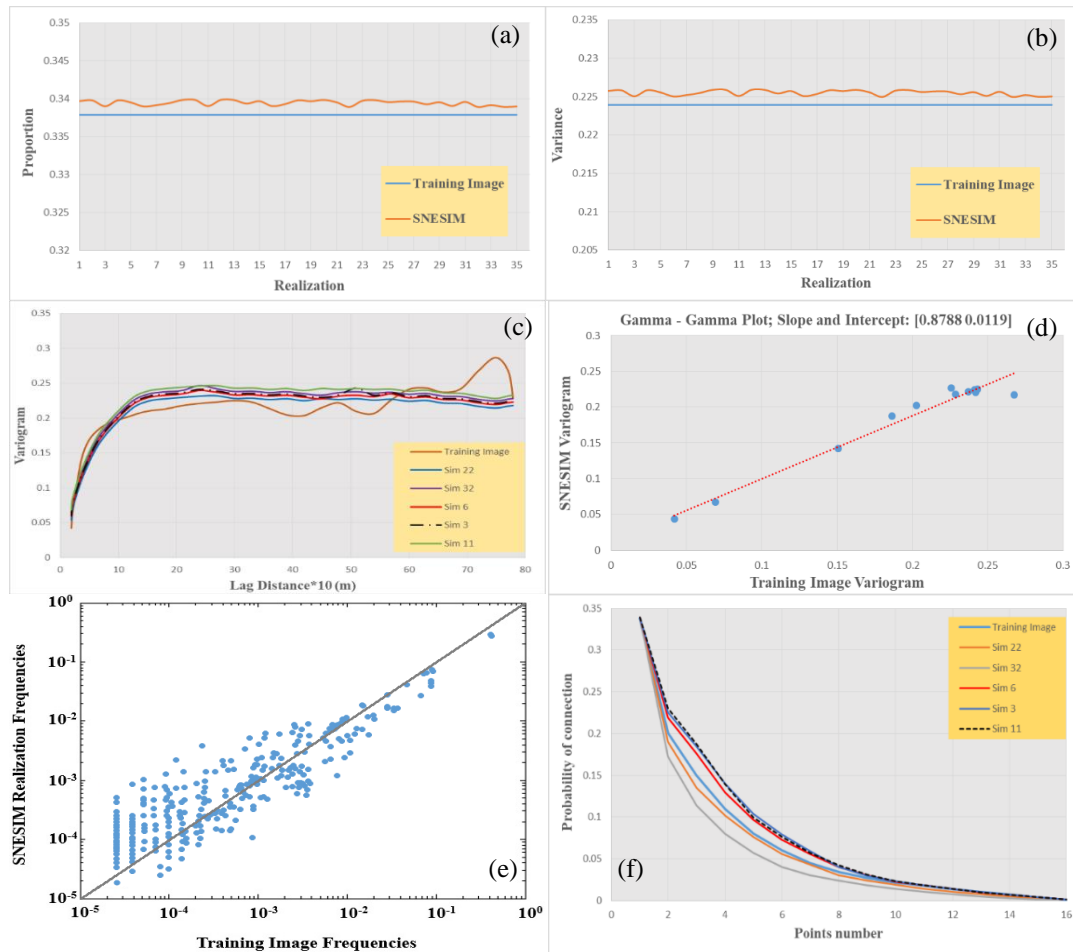


Figure 15. Graphical comparison of the single-point statistics parameters of the TI and SNESIM realizations, (a) proportion, (b) variance. Omni-directional variogram of five realizations and TI for deep region (c), Gamma-Gamma plot of the realization #22 than TI (d), frequency chart of reproduced patterns on the realization #22 and TI (e), and probability value of connectivity reproduction of the SNESIM realizations and TI (f).

Table 7. MSE and correlation results of Cumulants using the considered patterns (for part of the realizations).

Considered pattern	Realization number	Mean squared error	Correlation
{315, 45}	22	145×10^{-7}	0.901
	32	162×10^{-7}	0.854
	6	193×10^{-7}	0.794
	3	177×10^{-7}	0.824
	11	201×10^{-7}	0.781
{135, 135}	22	112×10^{-7}	0.937
	32	125×10^{-7}	0.921
	6	137×10^{-7}	0.915
	3	142×10^{-7}	0.894
{315, 135}	11	164×10^{-7}	0.842
	22	157×10^{-7}	0.854
	32	191×10^{-7}	0.789
	6	172×10^{-7}	0.801
{315, 135, 45}	3	207×10^{-7}	0.741
	11	224×10^{-7}	0.724
	22	201×10^{-6}	0.872
	32	217×10^{-6}	0.856
{135, 135, 135}	6	231×10^{-6}	0.839
	3	234×10^{-6}	0.834
	11	300×10^{-6}	0.712
	22	146×10^{-6}	0.894
{135, 135, 135}	32	174×10^{-6}	0.841
	6	197×10^{-6}	0.812
	3	212×10^{-6}	0.794
	11	315×10^{-6}	0.723

Table 8. Final results obtained by the VIKOR method for deeper portions of the Sungun deposit.

Realization number	S	R	Q	Rating
22	0.018	0.138	0.059	1
32	0.077	0.147	0.124	2
6	0.065	0.247	0.165	3
3	0.048	0.373	0.214	4
11	0.096	0.293	0.221	5
21	0.082	0.327	0.225	6
18	0.245	0.243	0.346	7
13	0.091	0.681	0.422	8
14	0.461	0.056	0.467	9
2	0.337	0.301	0.471	10
16	0.409	0.208	0.494	11
26	0.386	0.253	0.495	12
25	0.120	0.881	0.557	13
33	0.537	0.111	0.574	14
27	0.536	0.184	0.612	15
1	0.142	0.949	0.616	16
4	0.328	0.595	0.618	17
30	0.390	0.494	0.627	18
35	0.364	0.688	0.703	19
34	0.508	0.522	0.762	20
7	0.799	0.051	0.809	21
15	0.879	0.066	0.898	22
28	0.425	0.969	0.915	23
5	0.579	0.707	0.933	24
17	0.800	0.386	0.987	25
8	0.991	0.027	0.992	26
12	0.666	0.657	0.995	27
20	0.651	0.750	1.029	28
10	0.763	0.556	1.040	29
31	0.690	0.802	1.096	30
29	0.760	0.835	1.185	31
19	0.722	0.946	1.205	32
23	0.985	0.622	1.301	33
24	0.865	0.953	1.355	34
9	0.999	0.720	1.368	35

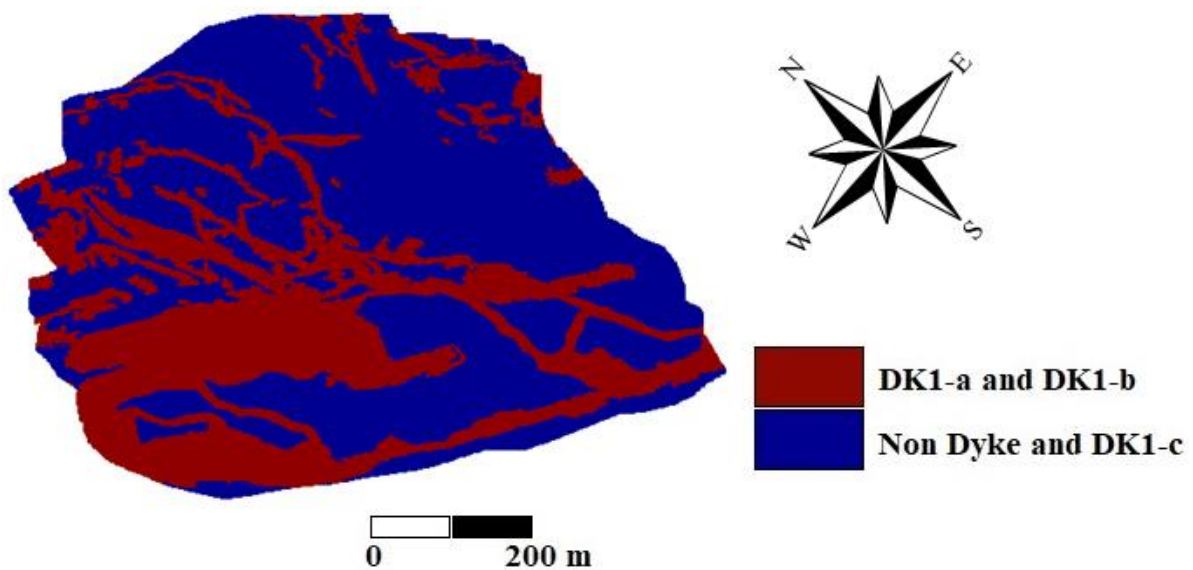


Figure 16. A 3D view of the best realization #22 through running the SNESIM method at the deeper portions of the Sungun deposit.

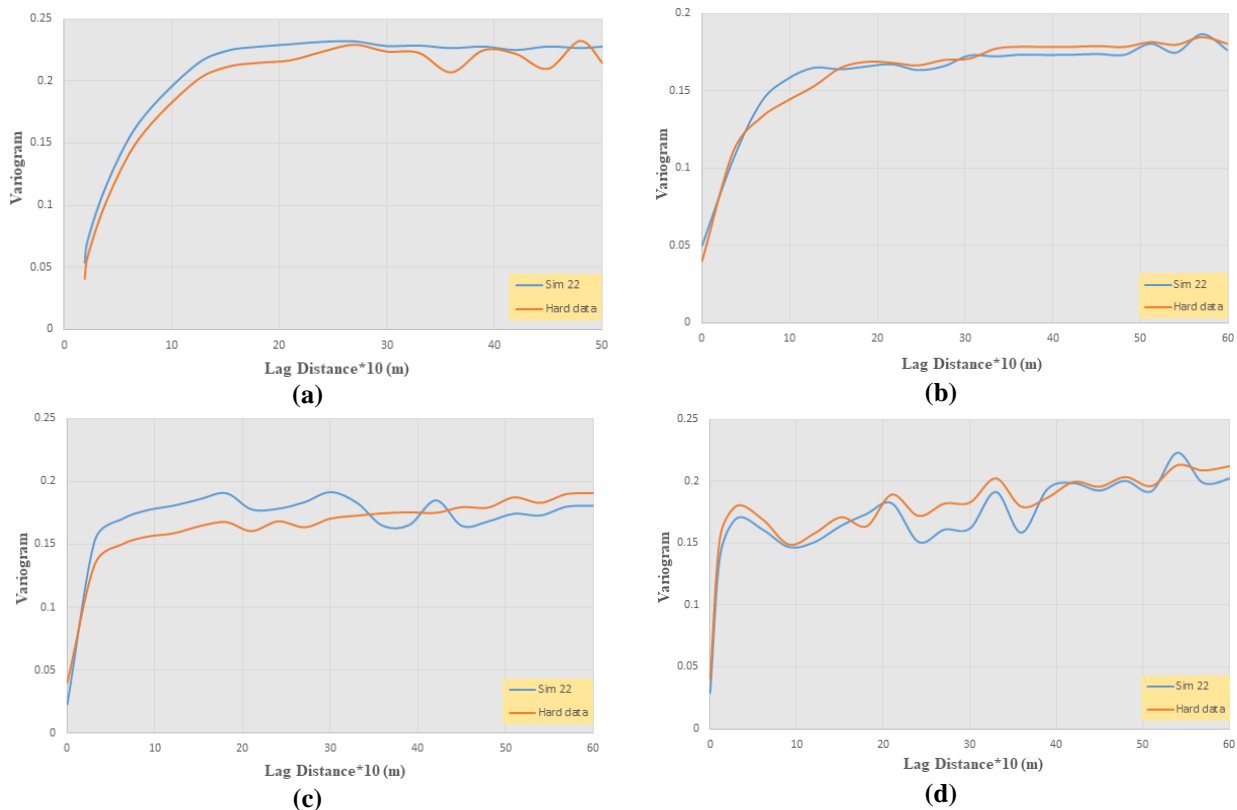


Figure 17. Variogram models of the best realization #22 and hard data, (a) Omni-directional, (b) Azimuth 315 and dip 67.5, (c) Azimuth 135 and dip 22.5, and (d) Azimuth 45 and dip 0.

5. Conclusions

This work was an attempt to model dyke structures of Sungun using a multi-step SNESIM algorithm. To this end, the MCDM and MPS approaches were used in a combined form. In the first step, a training image was constructed from the surface geological map to simulate an upper portion of the Sungun porphyry-Cu deposit. After simulation of shallow depth, several statistical criteria of realizations and TI were compared as well to select a new TI. Various statistical criteria such as single-point statistics, two-point statistics, multiple-point statistics, connectivity reproduction, and high order covariance reproduction (Cumulants) were incorporated in a MCDM problem to choose the best realization of simulation. Then the weight of statistical criteria was incorporated through a novel AHP-BMW approach to differentiate their importance in the final decision-making. In the next step, the VIKOR method was used to select the best realization of shallow depth results. The best realization was used as TI to generalize dyke simulation in the deeper portion of the studied region. Finally, Similar to the previous section, the realizations obtained from SNESIM algorithm in the deep region were sorted based on the several statistical criteria and AHP-BMW results.

References

- [1]. Chatterjee, S., Mustapha, H. and Dimitrakopoulos, R. (2016). Fast wavelet-based stochastic simulation using training images. *Computational Geosciences*. 20 (3): 399-420.
- [2]. Deutsch, C.V. and Journel, A.G. (1998). *GSLIB Geostatistical software library and user's guide*; Oxford University Press, New York.
- [3]. Sinclair, A.J. and Blackwell, G.H. (2002). *Applied mineral inventory estimation*. Cambridge University Press.
- [4]. Blackwell, G.H., Anderson, M. and Ronson, K. (1999). Simulated grades and open pit mine planning—resolving opposed positions. In *Proc. 28th Symp. On Application of computers and operations research to the minerals industry*, Colorado School of Mines, Golden, Colo, pp. 205-215.
- [5]. Caers, J. and Zhang, T. (2004). Multiple-point geostatistics: a quantitative vehicle for integrating geologic analogs into multiple reservoir models, Vol. 112, pp.213-234.
- [6]. Guardiano, F.B. and Srivastava, R.M. (1993). Multivariate geostatistics: beyond bivariate moments. In *Geostatistics Troia'92* (pp. 133-144). Springer, Dordrecht.

- [7]. Tran, T.T. (1994). Improving variogram reproduction on dense simulation grids. *Computers & Geosciences*, 20(7-8): 1161-1168.
- [8]. Roberts, E.S. (1998). Programming abstractions in C: A second course in computer science: AddisonWesley, Reading, MA, 819 p.
- [9]. Strebelle, S. (2000). Sequential simulation drawing structure from training images. Ph.D. Thesis, Stanford University, Stanford, CA, USA.
- [10]. Caers, J. (2001). Geostatistical reservoir modelling using statistical pattern recognition. *Journal of Petroleum Science and Engineering*. 29 (3-4): 177-188.
- [11]. Journel, A.G. (2002). Combining knowledge from diverse sources: An alternative to traditional data independence hypotheses. *Mathematical geology*. 34 (5): 573-596.
- [12]. Zhang, T. and Journel, A. (2002). Merging prior structural interpretation and local data: the multiple-point geostatistics answer. Stanford Center for Reservoir Forecasting Annual Report 16. Stanford University, Stanford, CA.
- [13]. Arpat, B.G. (2004). Sequential simulation with patterns, Ph.D. thesis, Stanford University, Stanford, CA., USA.
- [14]. Arpat, G.B. and Caers, J. (2007). Conditional simulation with patterns. *Mathematical Geology*. 39 (2): 177-203.
- [15]. Strebelle, S. (2002). Conditional simulation of complex geological structures using multiple-point statistics. *Mathematical Geology*. 34 (1): 1-21.
- [16]. Remy, N., Journel, A.G., Boucher, A. and Wu, J. (2007). Stanford Geostatistics Modeling Software.
- [17]. Zhang, T. (2006). Filter-based Training Pattern Classification for spatial pattern Simulation, Ph.D. thesis, Stanford University, Stanford, CA., USA.
- [18]. Wu, J., Boucher, A. and Zhang, T. (2008). A SGeMS code for pattern simulation of continuous and categorical variables: FILTERSIM. *Computers & Geosciences*. 34 (12): 1863-1876.
- [19]. Mariethoz, G., Renard, P. and Straubhaar, J. (2010). The direct sampling method to perform multiple-point geostatistical simulations. *Water Resources Research*. 46 (11).
- [20]. Tahmasebi, P., Hezarkhani, A. and Sahimi, M. (2012). Multiple-point geostatistical modeling based on the cross-correlation functions. *Computational Geosciences*. 16 (3): 779-797.
- [21]. Abdollahifard, M.J. and Faez, K. (2013). Stochastic simulation of patterns using Bayesian pattern modeling. *Computational Geosciences*. 17 (1): 99-116.
- [22]. Faucher, C., Saucier, A. and Marcotte, D. (2013). A new patchwork simulation method with control of the local-mean histogram. *Stochastic environmental research and risk assessment*. 27 (1): 253-273.
- [23]. Tahmasebi, P., Sahimi, M. and Caers, J. (2014). MS-CCSIM: accelerating pattern-based geostatistical simulation of categorical variables using a multi-scale search in Fourier space. *Computers & Geosciences*, 67: 75-88.
- [24]. Moura, P., Laber, E., Lopes, H., Mesejo, D., Pavanelli, L., Jardim, J., Thiesen, F. and Pujol, G. (2017). LSHSIM: A Locality Sensitive Hashing based method for multiple-point geostatistics. *Computers & Geosciences*, 107: 49-60.
- [25]. Bavand Savadkoohi, M., Tokhmechi, B., Gloaguen, E. and Arab-Amiri, A.R., 2019. A comprehensive benchmark between two filter-based multiple-point simulation algorithms. *Journal of Mining and Environment*. 10 (1): 139-149.
- [26]. Rezaee, H., Asghari, O., Koneshloo, M. and Ortiz, J.M. (2014). Multiple-point geostatistical simulation of dykes: application at Sungun porphyry copper system, Iran. *Stochastic environmental research and risk assessment*, 28(7): 1913-1927.
- [27]. Rezaee, H., Mariethoz, G., Koneshloo, M. and Asghari, O. (2013). Multiple-point geostatistical simulation using the bunch-pasting direct sampling method. *Computers & Geosciences*, 54: 293-308.
- [28]. Hashemi, S., Javaherian, A., Ataee-pour, M., Tahmasebi, P. and Khoshdel, H. (2014). Channel characterization using multiple-point geostatistics, neural network, and modern analogy: A case study from a carbonate reservoir, southwest Iran. *Journal of Applied Geophysics*, 111: 47-58.
- [29]. Tuanfeng, Z. (2008). Incorporating Geological Conceptual Models and Interpretations into Reservoir Modeling Using Multiple-Point Geostatistics, *Earth Science Frontiers*. 15 (1): 26 - 35.
- [30]. Lai, Y.J., Liu, T.Y. and Hwang, C.L. (1994). Topsis for MODM. *European journal of operational research*, 76(3): 486-500.
- [31]. Deng, H., Yeh, C.H. and Willis, R.J. (2000). Inter-company comparison using modified TOPSIS with objective weights. *Computers & Operations Research*. 27 (10): 963-973.
- [32]. Li, D.F. and Yang, J.B. (2004). Fuzzy linear programming technique for multiattribute group decision making in fuzzy environments. *Information Sciences*, 158: 263-275.
- [33]. Li, D.F. 2005. Multiattribute decision making models and methods using intuitionistic fuzzy sets. *Journal of computer and System Sciences*. 70 (1): 73-85.
- [34]. Opricovic, S. and Tzeng, G.H. (2004). Compromise solution by MCDM methods: A

comparative analysis of VIKOR and TOPSIS. European journal of operational research. 156 (2): 445-455.

[35]. Opricovic, S. and Tzeng, G.H. (2007). Extended VIKOR method in comparison with outranking methods. European journal of operational research, 178(2): 514-529.

[36]. Rezaei, J. (2015). Best-worst multi-criteria decision-making method. Omega, 53: 49-57.

[37]. Feng, W. and Wu, S. (2016). A multiple-point geostatistical method based on geological vector information. Arabian Journal of Geosciences. 9 (10): 562.

[38]. Huang, T., Lu, D.T., Li, X. and Wang, L. (2013). GPU-based SNESIM implementation for multiple-point statistical simulation. Computers & Geosciences, 54: 75-87.

[39]. Yang, L., Hou, W., Cui, C. and Cui, J. (2016). GOSIM: a multi-scale iterative multiple-point statistics algorithm with global optimization. Computers & Geosciences, 89: 57-70.

[40]. Saaty, T.L. (1977). A scaling method for priorities in hierarchical structures. Journal of mathematical psychology, 15(3): 234-281.

[41]. Boroushaki, S. and Malczewski, J. (2008). Implementing an extension of the analytical hierarchy process using ordered weighted averaging operators with fuzzy quantifiers in ArcGIS. Computers and Geosciences, 34: 399-410.

[42]. Hajkiewicz, S., Young, M. and MacDonald, D.H. (2000). Supporting decisions: Understanding natural resource management assessment techniques (No. 00_003). Policy and Economic Research Unit, CSIRO Land and Water, Adelaide, Australia.

[43]. Rezaei, J. (2016). Best-worst multi-criteria decision-making method: Some properties and a linear model. Omega, 64: 126-130.

[44]. Mohaghar, A., Sahebi, I.G. and Arab, A. (2017). Appraisal of humanitarian supply chain risks using best-worst method. International Journal of Social, Behavioral, Educational, Economic, Business and Industrial Engineering. 11 (2): 309-314.

[45]. Torabi, S.A., Giahi, R. and Sahebjamnia, N. (2016). An enhanced risk assessment framework for business continuity management systems. Safety science, 89: 201-218.

[46]. Hosseinali, F. and Alesheikh, A.A. (2008). Weighting spatial information in GIS for copper mining exploration. American Journal of Applied Sciences, 5: 1187-1198.

[47]. Lee, A.H.I., Chen, W.C. and Chang, C.J. (2008). A fuzzy AHP and BSC approach for evaluating performance of IT department in the manufacturing industry in Taiwan. Expert Systems with Applications, 34: 96-107.

[48]. San Cristóbal, J.R. (2011). Multi-criteria decision-making in the selection of a renewable energy project in Spain: The Vikor method. Renewable energy. 36 (2): 498-502.

[49]. Rezaie, K., Ramiyani, S.S., Nazari-Shirkouhi, S. and Badizadeh, A. (2014). Evaluating performance of Iranian cement firms using an integrated fuzzy AHP-VIKOR method. Applied Mathematical Modelling. 38 (21-22): 5033-5046.

[50]. Gupta, P., Mehlawat, M.K. and Grover, N. (2016). Intuitionistic fuzzy multi-attribute group decision-making with an application to plant location selection based on a new extended VIKOR method. Information Sciences, 370: 184-203.

[51]. Shokr, I., Amalnick, M.S. and Torabi, S.A. (2016). An Augmented Common Weight Data Envelopment Analysis for Material Selection in High-tech Industries. International Journal of Supply and Operations Management. 3 (2): 1234.

[52]. Mousavi, S.M., Torabi, S.A. and Tavakkoli-Moghaddam, R. (2013). A hierarchical group decision-making approach for new product selection in a fuzzy environment. Arabian Journal for Science and Engineering, 38(11): 3233-3248.

[53]. Hezarkhani, A. and Williams-Jones, A.E. (1998). Controls of alteration and mineralization in the Sungun porphyry copper deposit, Iran: Evidence from fluid inclusions and stable isotopes. Economic Geology, 93: 651 - 670.

[54]. Mehrpartou, M. (1993). Contributions to the geology, geochemistry, Ore genesis and fluid inclusion investigations on Sungun Cu-Mo porphyry deposit, northwest of Iran. PhD Thesis. University of Hamburg, Germany.

[55]. Hezarkhani, A., Williams-Jones, A.E. and Gammons, C.H. (1999). Title of subordinate document. In: Factors controlling copper solubility and chalcopyrite deposition in the Sungun porphyry copper deposit, Iran. Mineralium deposita, 34: 770 - 783.

[56]. Calagari, A.A. (2004). Geochemical, stable isotope, noble gas, and fluid inclusion studies of mineralization and alteration at Sungun porphyry copper deposit, East Azarbaijan, Iran: Implication for genesis. Ph.D. thesis, Manchester University, Manchester, England.

[57]. Liu, Y. (2006). Using the snesim program for multiple-point statistical simulation, Computers & Geosciences, 32: 1544 - 1563.

[58]. Peredo, O. and Ortiz, J.M. (2011). Parallel implementation of simulated annealing to reproduce multiple-point statistics, Computers & Geosciences, 37: 1110 - 1121.

[59]. Journel, A.G. and Alabert, F.A. (1989). Non-Gaussian data expansion in the Earth Sciences, In Terra Nova, 1: 123 - 134.

[60]. Dimitrakopoulos, R., Mustapha, H. and Gloaguen, E. (2010). High-order statistics of spatial random fields: exploring spatial Cumulants for modeling complex non-Gaussian and non-linear phenomena. Mathematical Geosciences. 42 (1): 65.

[61]. De Iaco, S. and Maggio, S. (2011). Validation techniques for geological patterns simulations based on

variogram and multiple-point statistics. Mathematical Geosciences. 43 (4): 483-500.

[62]. Greco, S., Figueira, J. and Ehrgott, M. (2016). Multiple criteria decision analysis. New York: Springer.

[63]. Tzeng, G.H. and Huang, J.J. (2011). Multiple attribute decision making: methods and applications. Chapman and Hall/CRC.

یک انتخاب بهینه از مدل‌های شبیه‌سازی زمین‌شناسی با استفاده از رویکردهای زمین‌آماری چند نقطه‌ای و تصمیم‌گیری چند معیاره؛ یک مطالعه موردی در کانسار مس پورفیری سونگون، ایران

سجاد طالاش حسینی^۱، امید اصغری^{۱*}، سید علی ترابی^۲ و میثم عابدی^۳

۱- آزمایشگاه شبیه‌سازی و پردازش داده، دانشکده مهندسی معدن، پردیس دانشکده فنی، دانشگاه تهران، تهران، ایران

۲- دانشکده مهندسی صنایع، دانشکده مهندسی معدن، پردیس دانشکده فنی، دانشگاه تهران، تهران، ایران

۳- آزمایشگاه ژئوفیزیک اکتشافی، دانشکده مهندسی معدن، پردیس دانشکده فنی، دانشگاه تهران، تهران، ایران

ارسال ۲۰۱۹/۰۷/۱۹، پذیرش ۲۰۲۰/۰۲/۲۱

* نویسنده مسئول مکاتبات: o.asghari@ut.ac.ir

چکیده:

مدل‌سازی دقیق واحدهای زمین‌شناسی پیچیده تأثیر قابل توجهی در طراحی یک طرح استخراج معدن دارد. رویکردهای شبیه‌سازی زمین‌آماري، از طریق تعریف یک مدل واریوگرام یا تفسیر یک تصویر آموزشی (TI)، می‌توانند هنگام در دسترس بودن یک الگوی پراکنده از حفاری، واحدهای زمین‌شناسی مختلف را بازتولید کنند. تکنیک‌های مبتنی بر واریوگرام (حاصل از زمین‌آمارهای دونقطه‌ای) معمولاً از بازتولید واحدهای زمین‌شناسی پیچیده و غیرخطی رنج می‌برد. در حالی که، زمین‌آمار چند نقطه‌ای (MPS) این مشکل را با تفسیر تصویر آموزشی حاصل از اطلاعات زمین‌شناسی قبلی حل می‌کند. این مطالعه به بررسی ساختارهای دایک سیستم مس پورفیری در شمال غربی ایران، با استفاده از الگوریتم شبیه‌سازی معادله نرمال منفرد چند مرحله‌ای (SNESIM) می‌پردازد. به منظور انجام یک الگوریتم اسنسیم چند مرحله‌ای، رویکردهای زمین‌آماري چند نقطه‌ای و تصمیم‌گیری چند معیاره به صورت ترکیبی استفاده می‌شوند. برای این منظور، دو تصویر آموزشی، یکی برای شبیه‌سازی ساختارهای دایک در عمق کم و دیگری برای شبیه‌سازی ساختارهای دایک در عمق زیاد، در نظر گرفته شده است. در مرحله اول، یک تصویر آموزشی با استفاده از نقشه زمین‌شناسی استخراج شده در طی عملیات اکتشافی قبلی تولید می‌شود. پس از تولید تصویر آموزشی، ۳۵ تحقق برای عمق کم کانسار مورد مطالعه شبیه‌سازی می‌شود. برای انتخاب بهترین تحقق از نتایج شبیه‌سازی (به عنوان یک تصویر آموزشی برای مرحله بعد)، چندین معیار آماری استفاده و نتایج به دست آمده با هم مقایسه شدند. برای این هدف، یک روش تصمیم‌گیری چند معیاره هیبریدی براساس گروهی از معیارهای آماری طراحی شد. در مرحله بعد، ساختارهای دایک در عمق زیاد با استفاده از تصویر آموزشی جدید همچنین شبیه‌سازی شدند.

کلمات کلیدی: واحدهای زمین‌شناسی پیچیده، تصویر آموزشی، الگوریتم اسنسیم، تصمیم‌گیری چند معیاره، کانسار مس پورفیری سونگون.